Author(s): Lehikoinen, Antti & Arkkio, Antero

Title: Efficient Finite Element Computation of Circulating Currents in Thin Parallel Strands

Year: 2015

Version: Post print

Please cite the original version:

Lehikoinen, Antti & Arkkio, Antero. 2015. Efficient Finite Element Computation of Circulating Currents in Thin Parallel Strands. IEEE Transactions on Magnetics. Volume 52, Issue 3. 4. 0018-9464 (printed). DOI: 10.1109/tmag.2015.2481934.

Efficient Finite Element Computation of Circulating Currents in Thin Parallel Strands

Antti Lehikoinen and Antero Arkkio

Aalto University, Dept. of Electrical Engineering and Automation, P.O. Box 13000, FI-00076 Espoo, Finland

Electrical machines often utilize stranded parallel conductors to reduce the skin-effect losses. This practice can lead to uneven total current distribution among the strands, increasing the resistive losses. Direct finite element analysis of circulating current problems can be computationally costly due to the large number of nodal unknowns in the finite element mesh in the conductor domains. Methods to reduce the computational burden exist for special problems only. This paper proposes two efficient finite element formulations to solve circulating current problems with arbitrary winding configurations. According to simulations, the proposed methods yield reasonably accurate results significantly faster than the traditional brute-force approach.

***Index Terms*—Approximation methods, eddy currents, finite element analysis, proximity effects.**

I. Introduction

In random-wound electrical machines, windings are often divided into thin parallel strands to reduce the skin-effect losses. However, stranding conductors like this can lead to currents circulating between the parallel strands, occasionally almost doubling the resistive stator losses. Surprisingly little attention has been paid to finite element (FE) analysis of these circulating currents, mainly due to the long computation times resulting from finely meshing a large number of thin strands [1], [2]. Indeed, approaches have been mostly limited to analytical methods [3]–[5]. Where FE analysis has been performed, it has focused on machines with large form-wound conductors [6]–[8].

To reduce the computation times, stranded conductors have traditionally been modelled either as a large solid conductor with a uniform equivalent current density [9], or homogenized in the frequency- or time-domain [10]–[14]. Obviously, the first approach fails to model the circulating currents at all. Similarly, practically all work on homogenization has focused purely on the skin- and proximity effects, assuming all strands to be series-connected or restricting the analysis to Litz wires [15], [16].

This paper presents two alternative FE formulations to calculate the circulating currents in stranded windings of arbitrary configuration. The methods place no demands on the structure or refinement-level of the mesh used. The speed and accuracy of the proposed methods are evaluated on two test problems. According to the simulations, the methods yield reasonably accurate solutions significantly faster than the brute-force approach.

Manuscript received June 24, 2015; revised August 25, 2015; accepted September 20. Corresponding author: A. Lehikoinen (email: antti.lehikoinen@aalto.fi).
Color versions of one or more of the figures in this paper are available online at http://ieeexplore.ieee.org.
Digital Object Identifier 10.1109/TMAG.2015.2481934

II. Methods

A 2D eddy-current problem with N_s strands and N_i current loops can be described by the vector potential formulation

$$-\nabla\cdot(\nu\nabla A)+\frac{\partial}{\partial t}\sigma A-\sum_{l=1}^{N_\mathrm{s}}\frac{1}{l_\mathrm{e}}\sigma u_l=0 \tag{1}$$

$$u_l=R_l\sum_{k=1}^{N_\mathrm{i}}\eta\left(k,l\right)i_k+R_l\int_{D_l}\frac{\partial}{\partial t}\sigma A\,\mathrm{d}D_l,\ l=1\ldots N_\mathrm{s} \tag{2}$$

$$U_k=R^\mathrm{ew}i_k+\sum_{l=1}^{N_\mathrm{s}}\eta\left(k,l\right)u_l,\ k=1\ldots N_\mathrm{i}\,, \tag{3}$$

where u_l are the voltages over the strands (interpreted as functions of position in the first equation), $\eta\left(k,l\right)$ indicates if the strand l belongs to the current path k, and D_l is the domain of the strand l [6]. U_k is the supply voltage of the path k. R_l and R^ew are the strand and end-winding resistances, respectively, whereas ν and σ denote the material reluctivity and conductivity. Finally, l_e is the equivalent problem domain length in the z-direction.

Using the Galerkin approach yields the following block matrix equation

$$\begin{bmatrix}\mathbf{S}^\mathrm{AA}+\mathbf{M}\frac{\partial}{\partial t} & \mathbf{S}^\mathrm{Au} & \mathbf{0}\\ \mathbf{M}^\mathrm{uA}\frac{\partial}{\partial t} & -\mathbf{I} & \mathbf{R}^\mathrm{ui}\\ \mathbf{0} & \mathbf{R}^\mathrm{iu} & \mathbf{R}^\mathrm{ii}\end{bmatrix}\begin{bmatrix}\mathbf{A}\\ \mathbf{u}\\ \mathbf{i}\end{bmatrix}=\begin{bmatrix}\mathbf{0}\\ \mathbf{0}\\ \mathbf{U}\end{bmatrix}, \tag{4}$$

with the following block entries

$$\left[\mathbf{M}\right]_{r,c}=\int_{D_l}\sigma\varphi_r\varphi_c\,\mathrm{d}D_l,\ \left[\mathbf{S}^\mathrm{Au}\right]_{r,l}=\int_{D_l}-\frac{1}{l_\mathrm{e}}\sigma\varphi_r\,\mathrm{d}D_l$$
$$\left[\mathbf{M}^\mathrm{uA}\right]_{l,c}=R_l\int_{D_l}\sigma\varphi_c\,\mathrm{d}D_l \tag{5}$$

directly related to the strand l. Shape functions are denoted by φ. The remaining entries are defined in [6].

In the brute-force approach the strands are finely meshed to obtain accurate skin- and proximity-effect losses. However, it is the authors' hypothesis that this is not necessary for obtaining reasonably accurate total currents, provided that the strands are thin compared to the skin-depth. Thus, two alternative approaches are proposed, neither of them placing any demands on the fineness or structure of the mesh used.

1) In the *point-strand* method, the strands are assumed thin enough for the vector potential to be approximately constant over their area. Assuming that the strand l is centered on $\mathbf{x}_l$, (5) can be reduced to

$$\begin{aligned}
[\mathbf{M}]_{r,c} &\approx \sigma\varphi_r(\mathbf{x}_l)\varphi_c(\mathbf{x}_l)|D_l| = \frac{l_\mathrm{e}}{R_l}\varphi_r(\mathbf{x}_l)\varphi_c(\mathbf{x}_l) \\
\left[\mathbf{S}^{\mathrm{Au}}\right]_{r,l} &\approx -\frac{1}{R_l}\varphi_r(\mathbf{x}_l) \\
\left[\mathbf{M}^{\mathrm{uA}}\right]_{l,c} &\approx l_\mathrm{e}\varphi_c(\mathbf{x}_l).
\end{aligned} \tag{6}$$

These results follow immediately from the expression for the strand resistance

$$R_l = \frac{l_\mathrm{e}}{\sigma|D_l|}, \tag{7}$$

where $|D_l|$ is the cross-sectional area of strand l.

2) In the *polygon-strand* method, D_l are approximated with polygons but are otherwise unrestricted in size or shape. To evaluate the integrals in (5), the intersecting polygons of D_l and the mesh elements are first determined. Then, a background mesh is generated for these polygons. This mesh is only used for the integration, i.e. it does not result in additional nodal unknowns and is thus ignored in the solution step.

An example of the background mesh can be seen in Fig. 1. The strand is represented with the thick red polygon, while the FE mesh is drawn in black. The thick blue polygon illustrates the overlapping domain of the strand and a single FE mesh element. Finally, elements of the background mesh are presented with the thinner blue lines.

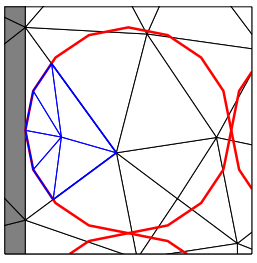

Fig. 1. Illustration of an auxiliary meshing.

With the background mesh, (5) can be evaluated with a slight modification to the well-known Gaussian quadrature approach based on reference elements. Let e be an element overlapping with the strand domain D_l, and k an background element belonging to e. Also, let F_e and $F^{\mathrm{bg}}_{e,k}$ be mappings from the reference element to the global element e and to the background element k, respectively. By slightly abusing this notation, the entries of e.g. $\mathbf{M}$ can be obtained with

$$\begin{aligned}
[\mathbf{M}]_{r,c} &= \int_{D_l} \sigma\varphi_r\varphi_c \,\mathrm{d}D_l = \\
&\sum_{e\in D_l}\sum_{k\in e}\sum_i w_i\hat{\varphi}_r\hat{\varphi}_c\left(F_e^{-1}F^{\mathrm{bg}}_{e,k}\left(\hat{\mathbf{x}}_i\right)\right)|\det\mathbf{J}\left(F^{\mathrm{bg}}_{e,k}\left(\hat{\mathbf{x}}_i\right)\right)|.
\end{aligned} \tag{8}$$

Here, $\hat{\mathbf{x}}_i$ and w_i are the integration points and weights for the reference element, whereas $\hat{\varphi}$ are the reference element shape functions and $\mathbf{J}$ is the Jacobian. The composition $F_e^{-1}F^{\mathrm{bg}}_{e,k}$ is used since $\hat{\varphi}$ are defined based on e, whereas the integration is performed over k. $\mathbf{S}^{\mathrm{Au}}$ and $\mathbf{M}^{\mathrm{uA}}$ can be obtained in a similar fashion.

Both methods can be extended to 3D problems relatively easily. In the point-strand method, the single point evaluation has to be replaced with a line integral. In the polygon-strand method, the intersection of polygons is replaced by an intersection of volumes, but the method remains otherwise effectively unchanged.

III. Simulation Results

The accuracy of the proposed methods was evaluated on two simple test problems. First-order elements were used, and the materials were assumed magnetically linear.

A. Inductor

Time-harmonic analysis was performed on an E-core inductor with 80 strands (1.7 mm in diameter) per slot and 4 parallel paths. Figs. 2a and 2b show the initial unrefined meshes used with the brute-force method and the proposed methods, with 1792 and 151 nodes respectively. 16-gons were used in the polygon-strand method. The winding configuration was intentionally naive to obtain large circulating currents.

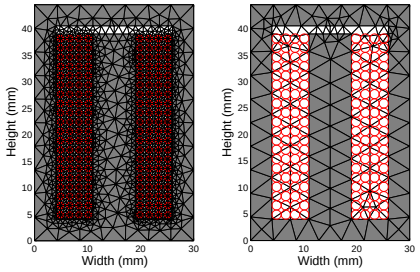

(a) (b)

Fig. 2. Initial unrefined meshes for the (a) brute-force and (b) proposed methods. Strands are highlighted with red.

To illustrate the potential accuracy of the proposed methods, Fig. 3 shows the behaviour of the four total current phasors on the complex plane, as the supply frequency was increased from 10 Hz (solid dot) to 1 kHz (empty dot). The solid lines were calculated with the brute-force method, while the dotted and dashed lines represent the point-strand and polygon-strand method, respectively. As can be seen, a good agreement between the methods was obtained.

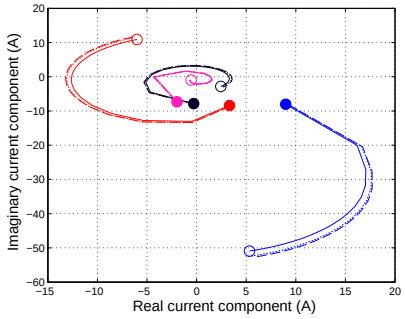

Fig. 3. Evolution of current phasors on the complex plane as frequency is increased from 10 Hz (solid dot) to 1 kHz (empty dot). Solid lines represent the brute-force method, and the dashed/dotted lines the proposed methods.

Furthermore, Fig. 4 illustrates the computation times and mean current errors of all three methods, obtained by repeating the simulations with different levels of *uniform* (non-adaptive) mesh refinement. Currents obtained with the brute-force method on a very dense mesh were used as reference values. Currents by the proposed methods fell within 20 % of the reference values at approximately 1/4000 of the computation cost, and within 5 % at 1/1000 of the cost. On dense meshes, the polygon-strand and brute-force method were roughly on par, whereas the point-strand method started to diverge. The diverging behaviour was probably caused by the fact that the strands were no longer small compared to the element size, so the approximations (6) became inaccurate.

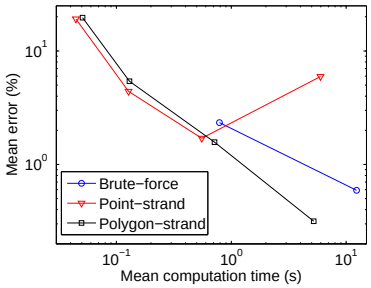

Fig. 4. Mean errors and computation times with different levels of non-adaptive mesh refinement.

B. Permanent Magnet Machine

To further evaluate the accuracy of the proposed methods, time-stepping analysis was performed on two slightly different four-pole permanent magnet (PM) machines rotating at 15 000 rpm, one with open and the other with semi-closed slots. Five electrical periods after synchronization at 0 s were simulated with 400 steps per period.

The main dimensions of the machines can be found in Table I. The machine with semi-closed slots has a slightly larger stator radius, but otherwise the dimensions are equal. The machines have a single-layer winding with three effective turns per slot, and 16 strands in parallel in each phase. A quarter of the machine cross-section is presented in Fig. 5. Phases and turns are emphasized with different colors and shadings, respectively.

TABLE I
MAIN DIMENSIONS OF THE PM MACHINE.

Winding connection	Delta
Number of turns	3
Number of parallel strands	16
Diameter of strands (mm)	1.25
Number of stator slots	36
Outer radius of stator (mm)	105 (108)
Inner radius of stator (mm)	70
Core length (mm)	200
PM height (mm)	8
Air-gap length (mm)	3

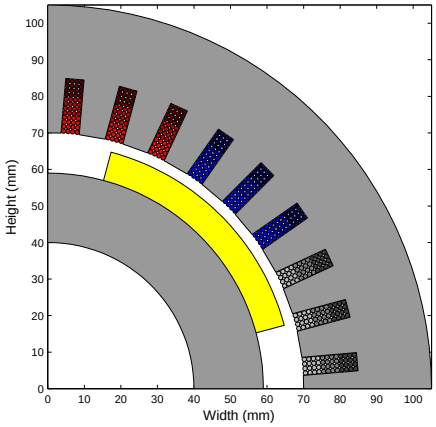

Fig. 5. A quarter of the machine cross-section.

The open-slotted machine was analysed first. Figs. 6a and 6b show the mesh over one slot pitch used with the brute-force and proposed methods, respectively. Fig. 7 shows the circulating current losses as a function of time [1]. The blue line denotes the results obtained with the brute-force method, while the two proposed methods are displayed with red and black. It can be seen that the two proposed methods gave almost equal results, both approximately 20 % larger than the brute-force method.

To improve accuracy, the mesh used with the proposed methods was refined inside the slots and the simulations were repeated. The refined mesh is illustrated in Fig. 6c. A comparison of the results can be found in Fig. 8, where the uppermost subfigure shows the initial results, while the results after the refinement can be seen in the middle one. Obviously, a significantly improved agreement was obtained between the brute-force and the proposed methods.

Furthermore, Table II shows the number of nodes in the mesh and the computation times. Even with the refined mesh, the proposed methods were more than seven times faster than the brute-force approach, while reaching a comparable accuracy.

The simulations were repeated for the machine with semi-closed stator slots. The slot mesh for the proposed methods is illustrated in Fig. 6d, while the simulation results can be found from the lowest subfigure of Fig. 8. This time, all three methods gave almost identical results. Computation times remained virtually the same as the ones in Table II.

TABLE II
SIMULATION DETAILS (OPEN-SLOTTED MACHINE).

	No. of nodes	Computation time (s)
Brute-force	5288	1052.7
Point-strand (unrefined)	442	129.5
Polygon-strand (unrefined)		124.7
Point-strand (refined)	938	153.2
Polygon-strand (refined)		158.3

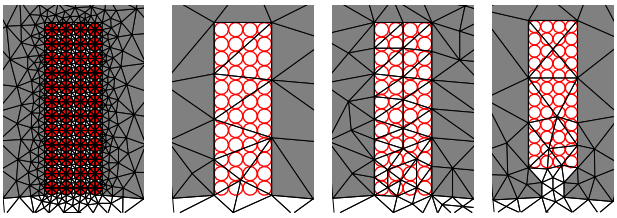

(a) (b) (c) (d)

Fig. 6. Illustrations of different slot-region meshes: (a) Brute-force method; open slots. (b) Unrefined mesh for the proposed methods; open slots. (c) Refined mesh for the proposed methods; open slots. (d) Proposed methods; semi-closed slots.

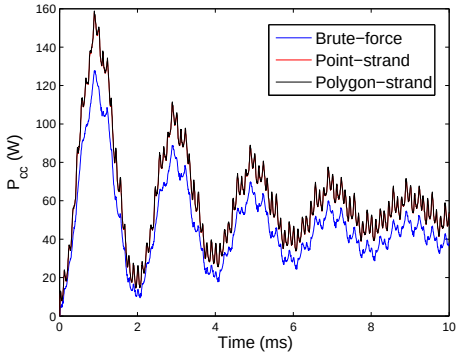

Fig. 7. Circulating current losses as function of time, obtained with the three methods.

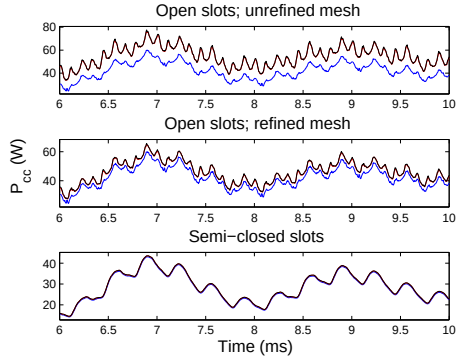

Fig. 8. Comparison of circulating current losses during the last two periods in different conditions.

IV. CONCLUSION

Two methods were presented for finite element computation of circulating currents in arbitrary windings. Based on simulations, both methods yield reasonably accurate results at a fractional computational cost compared to the brute-force approach. More importantly, arbitrarily coarse meshes can be used. This is a significant improvement over the brute-force method, where meshing requirements set a high lower bound for the number of nodal unknowns.

ACKNOWLEDGMENT

The research leading to these results has received funding from the European Research Council under the European Unions Seventh Framework Programme (FP7/2007-2013) / ERC Grant Agreement n. 339380.

REFERENCES

[1] J. Lähteenmäki, "Design and voltage supply of high-speed induction machines," Ph.D. dissertation, Helsinki University of Technology, Espoo, Nov 2002. [Online]. Available: http://lib.tkk.fi/Diss/2002/isbn951226224X/

[2] M. Islam, "Finite-element analysis of eddy currents in the form-wound multi-conductor windings of electrical machines," Ph.D. dissertation, Aalto University, Espoo, Jan 2010. [Online]. Available: http://lib.tkk.fi/Diss/2010/isbn9789522482556/

[3] J. Fang, X. Liu, B. Han, and K. Wang, "Analysis of circulating current loss for high speed permanent magnet motor," *IEEE Trans. Magn.*, 2014, to be published.

[4] X. Bian and Y. Liang, "Circuit network model of stator transposition bar in large generators and calculation of circulating current," *Industrial Electronics, IEEE Transactions on*, vol. 62, no. 3, pp. 1392–1399, March 2015.

[5] J. Yoshida, N. Hino, K. Takahashi, A. Nakahara, A. Komura, and K. Hattori, "Calculation method of circulating current in parallel armature windings in consideration of magnetic circuit," in *2013 IEEE Power and Energy Society General Meeting (PES)*, July 2013, pp. 1–5.

[6] M. Islam, J. Pippuri, J. Perho, and A. Arkkio, "Time-harmonic finite-element analysis of eddy currents in the form-wound stator winding of a cage induction motor," *IET Electric Power Applications*, vol. 1, no. 5, pp. 839–846, Sept 2007.

[7] X. Dexin, Y. Xiuke, Y. Yingying, B. Baodong, and N. Takahashi, "Circulating current computation and transposition design for large current winding of transformer with multi-section strategy and hybrid optimal method," *IEEE Trans. Magn.*, vol. 36, no. 4, pp. 1014–1017, Jul 2000.

[8] B. Baodong, X. Dexin, C. Jiefan, and O. Mohammed, "Optimal transposition design of transformer windings by genetic algorithms," *IEEE Trans. Magn.*, vol. 31, no. 6, pp. 3572–3574, Nov 1995.

[9] P. Lombard and G. Meunier, "A general purpose method for electric and magnetic combined problems for 2D, axisymmetric and transient systems," *IEEE Trans. Magn.*, vol. 29, no. 2, pp. 1737–1740, Mar 1993.

[10] Z. De Greve, O. Deblecker, J. Lobry, and J.-P. Keradec, "High-frequency multi-winding magnetic components: From numerical simulation to equivalent circuits with frequency-independent RL parameters," *IEEE Trans. Magn.*, vol. 50, no. 2, pp. 141–144, Feb 2014.

[11] J. Gyselinck, R. Sabariego, and P. Dular, "Time-domain homogenization of windings in 2-D finite element models," *IEEE Trans. Magn.*, vol. 43, no. 4, pp. 1297–1300, April 2007.

[12] R. Sabariego, P. Dular, and J. Gyselinck, "Time-domain homogenization of windings in 3-D finite element models," *IEEE Trans. Magn.*, vol. 44, no. 6, pp. 1302–1305, June 2008.

[13] J. Gyselinck, P. Dular, N. Sadowski, P. Kuo-Peng, and R. Sabariego, "Homogenization of form-wound windings in frequency and time domain finite-element modeling of electrical machines," *IEEE Trans. Magn.*, vol. 46, no. 8, pp. 2852–2855, Aug 2010.

[14] J. Gyselinck and P. Dular, "Frequency-domain homogenization of bundles of wires in 2-D magnetodynamic FE calculations," *IEEE Trans. Magn.*, vol. 41, no. 5, pp. 1416–1419, May 2005.

[15] J. Sibue, J. Ferrieux, G. Meunier, and R. Periot, "Modeling of losses and current density distribution in conductors of a large air-gap transformer using homogenization and 3-D FEM," *IEEE Trans. Magn.*, vol. 48, no. 2, pp. 763–766, Feb 2012.

[16] J.-R. Sibue, G. Meunier, J.-P. Ferrieux, J. Roudet, and R. Periot, "Modeling and computation of losses in conductors and magnetic cores of a large air gap transformer dedicated to contactless energy transfer," *IEEE Trans. Magn.*, vol. 49, no. 1, pp. 586–590, Jan 2013.